Vacuum referred binding energy of 3d transition metal ions for persistent and photostimulated luminescence phosphors of cerium-doped garnets

Ueda, Jumpei; Hashimoto, Atsunori; Takemura, Shota; Ogasawara, Kazuyoshi; Dorenbos, Pieter; Tanabe, Setsuhisa

DOI
10.1016/j.jlumin.2017.07.006

Publication date
2017

Document Version
Accepted author manuscript

Published in
Journal of Luminescence

Link to formal publication Journal of Luminescence (Elsevier): http://dx.doi.org/10.1016/j.jlumin.2017.07.006

Vacuum Referred Binding Energy of 3*d* Transition Metal Ions for Persistent and Photostimulated Luminescence Phosphors of Cerium-doped Garnet

Jumpei Ueda* [†], Atsunori Hashimoto[†], Shota Takemura[‡], Kazuyoshi Ogasawara[‡], Pieter Dorenbos[§], Setsuhisa Tanabe[†]

[†]Graduate School of Human and Environmental Studies, Kyoto University, Kyoto 606-8501, Japan

[‡]Department of Chemistry, Kwansei Gakuin University, 2-1 Gakuen, Sanda, Hyogo 669-1337, Japan

[§]Luminescence Materials Research Group (FAME-RST), Faculty of Applied Sciences, Delft University of Technology, 2629 JB Delft, Netherlands

ABSTRACT

The $Y_3Al_{5-x}Ga_xO_{12}$(YAGG):Ce^{3+}-Cr^{3+} persistent phosphor is one of the materials in which Cr^{3+} ions act as electron traps. The possibility of electron traps by other transition metal ions (TM^{3+}, TM= Sc, Ti, V, Cr, Fe) was investigated and those electron trap depth was compared with each other. In the TL glow curves, the YAGG:Ce^{3+} samples co-doped with different TM^{3+} ions show different TL glow peak temperatures (i.e. different electron trap depth). The estimated vacuum referred binding energy of TM^{2+} from the trap depth shows a zig-zag curve, which is found to be originated from the various 3*d* electron energy affected by a number of *d* electron, nuclear charge and crystal field splitting. Utilizing the obtained TM^{2+} zig-zag curve, a new persistent phosphor of $Y_3Al_2Ga_3O_{12}$:Ce^{3+}-Sc^{3+} and a photostimulated phosphor of $Y_3Al_2Ga_3O_{12}$:Ce^{3+}-V^{3+} were successfully developed.

1. Introduction

Phosphors related carrier (electron or hole) trapping and detrapping processes, such as persistent phosphors, photostimulated phosphors, storage phosphors and photochromic materials, have been attracting a great deal of interest. These materials have been studied for a variety of applications, for example luminous paints[1], imaging plates for X-ray detection[2], dosimeter[3, 4] and photochromic materials[5, 6]. The fundamental principles driving each of these phenomena are very similar to each other. In each, carriers (mainly electrons) are trapped into some defects and de-trapped by either light or heat. To design the phosphors related with electron trapping and detrapping proesses, it is important to understand the species of electron donors and acceptors, and its energy level location.

In 2013, we have developed novel persistent ceramic phosphors with a new combination of lanthanide luminescent centers and transition metal trap centers were developed in the $Y_3Al_{5-x}Ga_xO_{12}$ (x=2.5, 3, 3.5) garnet (YAGG) doped with Ce^{3+} and Cr^{3+}. The phosphors show Ce^{3+}:5*d*-4*f* green persistent luminescence (λ_{em} = 510 nm) for several hours after blue-light excitation[7]. In our following works, we demonstrated that Ce^{3+} ions are photo-oxidized and Cr^{3+} ions are photo-reduced by UV illumination from the thermoluminescence glow curves, vacuum referred binding energy diagram and the XANES measurement[7-11]. From these results, it is found that the Cr^{3+} ions can act as electron traps by changing their valence state to Cr^{2+} in YAGG host material. In many persistent phosphors developed after the $SrAl_2O_4:Eu^{2+}$-Dy^{3+}[1, 12, 13], the electron traps are usually formed by codoping with trivalent lanthanide ions (Ln^{3+}). It is reported that the electron trap depth depends on the energy gap between Ln^{2+} (electron trap level) zig-zag curve and bottom of the conduction band (CB)[14-16]. Thus, the persistent luminescence properties can be controlled by co-dopant of Ln^{3+}. Similarly, we predicted that the vacuum

referred biding energy (VRBE) of an electron in TM^{2+} with different *d* electrons shows a zig-zag curve. For the analysis of TM^{2+} electron trap level, the $Y_3Al_{5-x}Ga_xO_{12}:Ce^{3+}$-$TM^{3+}$ series were chosen because Ce^{3+} in $Y_3Al_{5-x}Ga_xO_{12}$ is good electron donor materials by UV and blue excitation due to the suitable relative energy location of Ce^{3+}:$5d_1$ excited state and the bottom of CB[9, 10] and photo-oxidized Ce^{3+} is a stable hole trapping center. In this study, the thermoluminescence (TL) glow curves of $Y_3Al_{5-x}Ga_xO_{12}$(YAGG):Ce^{3+} codoped with 3*d* transition metal ions were analyzed, and the obtained trap depth was found to be changed in different TM^{3+} codopants. From the VRBE diagram constructed from the experimental TL data and first principle calculations, we concluded that the TM^{3+} acts as the electron traps and its VRBE of TM^{2+} are affected by the number of *d* electrons, effective nuclear charge and crystal field splitting.

2. Experimental procedure

Polycrystalline ceramics of $Y_3Al_{5-x}Ga_xO_{12}$(YAGG):Ce^{3+} codoped with transition metal ions were synthesized by solid state reaction. The compositions of the prepared samples are $(Y_{0.995}Ce_{0.005})_3Al_{4.999-x}Ga_xTM_{0.001}O_{12}$ with x=0, 1, 2, 3, 4 (TM=Sc, V, Cr) and $(Y_{0.995}Ce_{0.005})_3Al_{1.999-x}Ga_3TM_{0.001}O_{12}$ (TM=Ti, Fe). For YAGG:Ce-TM (Sc, V, Cr), the chemicals Y_2O_3 (99.99 %), Al_2O_3 (99.99 %), Ga_2O_3 (99.99 %), CeO_2 (99.99 %), Sc_2O_3 (99.99), V_2O_5 (99.9%), Cr_2O_3 (99.9%) were used as starting materials. The powders were mixed by ball milling (Fritsch, Premium Line P-7) with ethanol and the obtained slurry was dried and pulverized. For YAGG:Ce-TM (Ti, Fe), the powders of Y_2O_3 (99.99 %), Al_2O_3 (99.99 %), Ga_2O_3 (99.99 %), CeO_2 (99.99 %) were mixed by ball milling (Fritsch, Premium Line P-7) with

ethanol. The obtained slurry was dried and pulverized, and then $TiCl_3$ (99.9%), $Fe_2(SO_4)_3 \cdot nH_2O$ solution was added and mixed well. The dried powders were pressed at 50 MPa into pellets sized 10 mm-ϕ x 2 mm thick. The pellets were sintered at 1600 °C for 24 h in air.

TL glow curves were measured using a PMT (Hamamatsu Photonics, R3896) with a 475 nm short-cut filter and a 600nm long cut filter for detecting only Ce^{3+} luminescence. The samples were mounted on a cryostat (Advanced Research Systems, Helitran LT3) in order to control the temperature. The samples were excited by UV excitation (250 nm ~ 400 nm) from a 300W Xe-lamp at 100K for 10 min and started to be heated with 10K/min. heating rate to 600K 10 min after stopping the excitation light. PersL decay curves were measured by the PMT with 475-600 nm transparent window by the filters after excitation of the Xe lamp with a 460 nm bandpass filter. Photostimulated luminescence was detected by a multi-channel monochromator (Ocean Optics, QE65PRO) with 980 nm infra-red (IR) laser stimulation after and before charging by UV excitation (250nm~400nm). The charge transfer energy from O^{2-} to TM^{3+} in $Y_3Al_5O_{12}$ was calculated by the discrete variational multielectron (DVME) method developed by Ogasawara[17] using TMO_6^{9-} cluster with lattice relaxation correction. The effective Madelung potential was produced by surrounding the cluster with point charges at external atomic sites. The configuration dependent correction (CDC) between the $3d^n$ and $3d^{n+1}L^{-1}$ was taken into account, where L^{-1} denotes a ligand hole.

3. Results

3.1. TL glow curves

Figure 1 shows the normalized TL glow curves of $Y_3Al_2Ga_3O_{12}:Ce^{3+}$-$TM^{3+}$(TM=Sc, Ti, V, Cr, Fe). As a reference data, TL glow curves of Ce^{3+}-singly-doped $Y_3Al_2Ga_3O_{12}$[11] and $Y_3Al_2Ga_3O_{12}:Ce^{3+}$-$Yb^{3+}$ are also shown. Main TL peak of $Y_3Al_2Ga_3O_{12}:Ce^{3+}$-$TM^{3+}$(TM=Sc, Ti, V, Cr, Fe) was observed at 319 K, 367 K, 444 K, 294 K and 218 K. The Ga content dependence of TL glow curve in $Y_3Al_2Ga_3O_{12}:Ce^{3+}$-$TM^{3+}$ (TM=Sc, V) are shown in Figure 2 and 3, respectively. The main TL peak is shifted to a higher temperature up to x=1 sample, and then to lower temperature with increasing Ga content. The TL peak temperatures for $Y_3Al_2Ga_3O_{12}:Ce^{3+}$-$TM^{3+}$ (TM=Sc, V, Cr) are listed in Table 1.

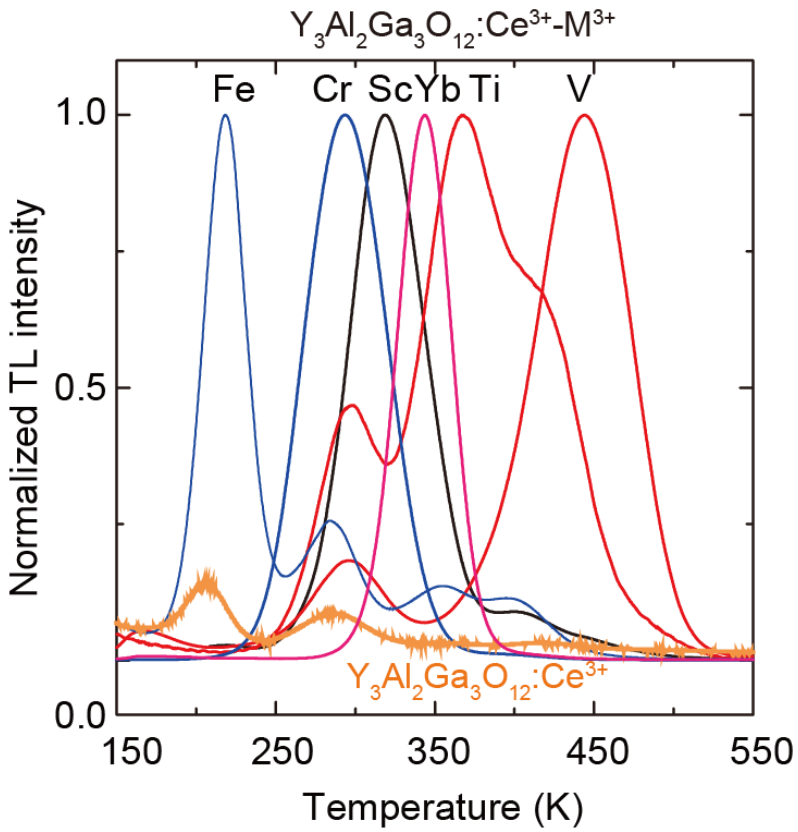

Figure 1. Normalized TL glow curves recorded with 10K/min heating rate of $Y_3Al_2Ga_3O_{12}:Ce^{3+}$-$TM^{3+}$(TM=Sc, Ti, V, Cr, Fe), $Y_3Al_2Ga_3O_{12}:Ce^{3+}$ -Yb^{3+} and $Y_3Al_2Ga_3O_{12}:Ce^{3+}$ after UV charging at 100 K.

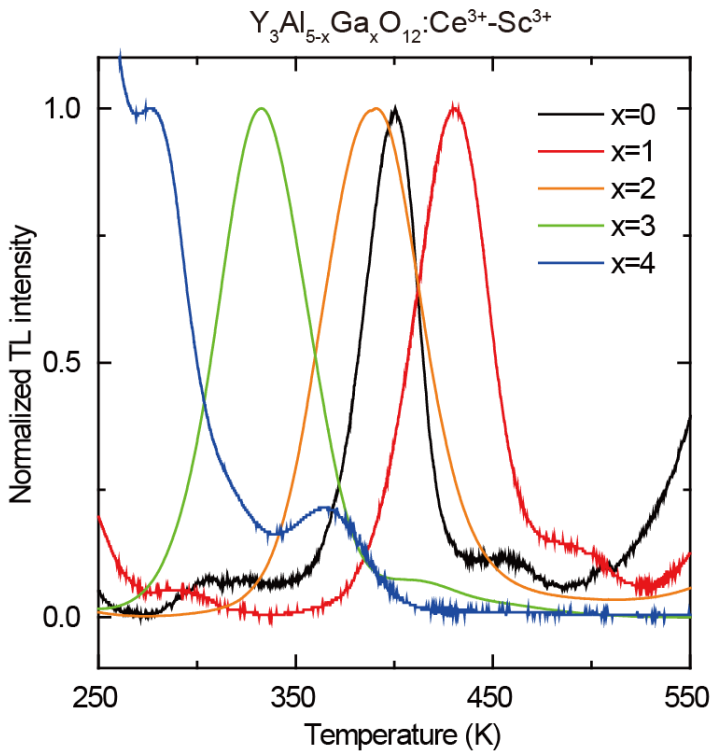

Figure 2. Normalized TL glow curves recorded at 10K/min heating rate of $Y_3Al_{5-x}Ga_xO_{12}:Ce^{3+}$-$Sc^{3+}$ with different Ga content x after UV charging at 100 K.

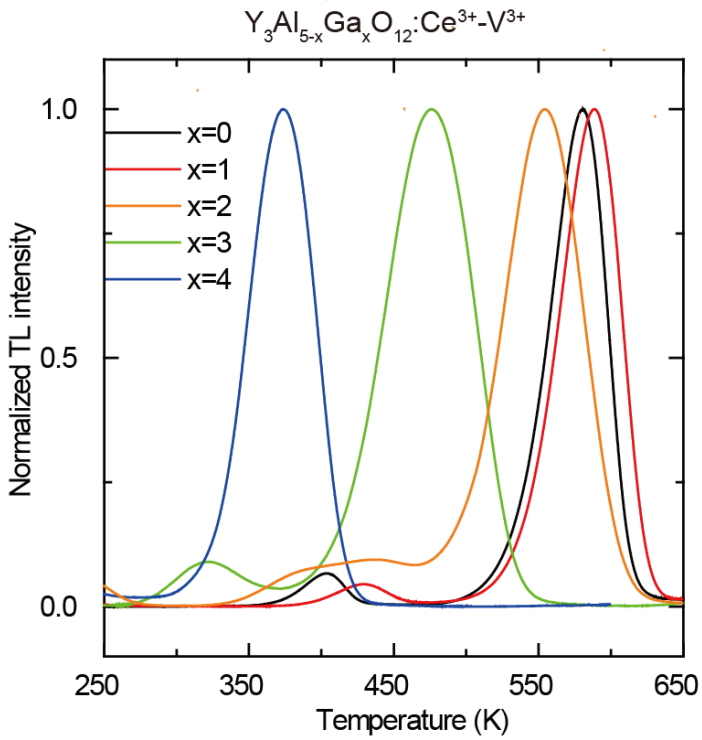

Figure 3. Normalized TL glow curves recorded at 10K/min heating rate of $Y_3Al_{5-x}Ga_xO_{12}:Ce^{3+}$-$V^{3+}$ with different Ga content x after UV charging at 100 K.

From the obtained TL glow peak temperature, the trap depth was estimated assuming first order kinetics and using Eq.(1) below[18, 19].

$$\frac{\beta E^{trap}}{kT_m{}^2} = s\exp(-\frac{E^{trap}}{kT_m}) \qquad (1).$$

Here, β is the heating rate (K/s), E^{trap} is trap depth, k is Boltzmann constant, T_m is a maximum temperature of TL glow peak, s is frequency factor. We already reported the frequency factor, s, in the $Y_3Al_{5-x}Ga_xO_{12}:Ce^{3+}$-$Cr^{3+}$ with different Ga content x by the heating rate analysis of TL glow curves[9]. Because the frequency factor usually depends on the host materials, the frequency factors in the $Y_3Al_{5-x}Ga_xO_{12}:Ce^{3+}$-$Cr^{3+}$ were used for the calculation of trap depth in $Y_3Al_{5-x}Ga_xO_{12}:Ce^{3+}$ samples with different codopants. The trap depth of the main TL glow peak in $Y_3Al_2Ga_3O_{12}:Ce^{3+}$ codoped with Sc^{3+}, Ti^{3+}, V^{3+}, Cr^{3+}, and Fe^{3+} is estimated to be 0.87, 0.96, 1.26, 0.81 and 0.56 eV, respectively. For the $Y_3Al_2Ga_3O_{12}:Ce^{3+}$-$Yb^{3+}$ as a reference, the observed TL peak temperature is 344 K, which corresponds to the 0.91 eV of trap depth. The TL peak temperature and the trap depth of the main TL glow peak in $Y_3Al_{5-x}Ga_xO_{12}:Ce^{3+}$-$TM^{3+}$ (TM=Sc, V, Cr) with different Ga content are shown in Table 1. The decline tendency of the trap depth for Ga content was observed.

Table 1. Temperature maximum, T_m, of TL glow curves recorded at 10 K min^{-1} heating rate, the trap depth, E^{trap}, and VRBE of Sc^{2+}, V^{2+} and Cr^{2+} (E_{Sc2+}, E_{V2+} and E_{Cr2+})

	T_m (K)			E^{trap} (eV)			E_{Sc2+}(eV)	E_{V2+} (eV)	E_{Cr2+} (eV)
	Sc	V	Cr	Sc	V	Cr			
x=0	401	580	384	1.23	1.80	1.02	-2.94	-3.51	-2.73
x=1	430	589	396	1.27	1.75	1.08	-2.91	-3.39	-2.72
x=2	391	554	343	1.14	1.64	1.02	-2.89	-3.39	-2.77
x=3	360	476	279	0.87	1.26	0.81	-2.86	-3.25	-2.80
x=4	(276)	374	214	0.69	0.95	0.56	-2.82	-3.08	-2.69

4. Discussion

4.1 VRBE of TM^{2+}

As shown in Figure 1, the TL peak temperature is dramatically changed by varying the codopant 3*d* transition metal ions. Also, it is entirely different from the small TL glow curve of $Y_3Al_2Ga_3O_{12}:Ce^{3+}$, which is possibly caused by the intrinsic defects. These results strongly suggest that the carrier trap is formed by 3*d* transition metal ion. Our previous results of XANES spectrum in $Y_3Al_2Ga_3O_{12}:Ce^{3+}$-$Cr^{3+}$ supports that the photoionized electron from Ce^{3+} moves to the Cr^{3+} after charging. Considering these results, other $3d^n$ transition metal ions are also likely to act as the electron traps and itself changes to $3d^{n+1}$ electron configuration.

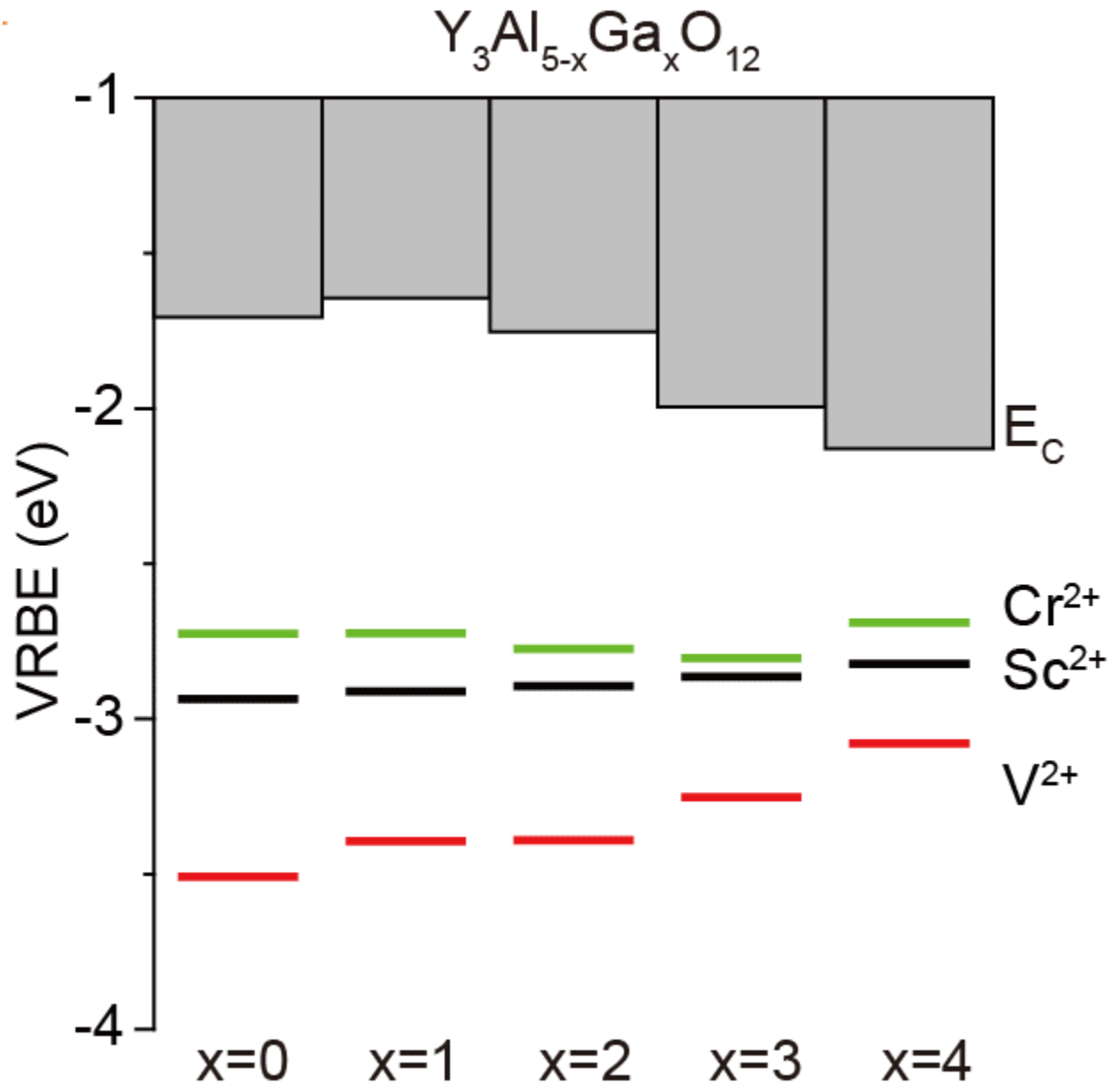

Figure 4. Stacked VRBE diagrams of $Y_3Al_{5-x}Ga_xO_{12}$ for TM^{2+} (TM=Sc, V, Cr).

Figure 4 shows the stacked vacuum referred binding energy of $Y_3Al_{5-x}Ga_xO_{12}$, which is constructed mainly using the parameter in our previous paper[9]. The VRBE of Sc^{2+}, V^{2+} and Cr^{2+} (E_{Sc2+}, E_{V2+}, E_{Cr2+}) level is plotted by subtracting the corresponding trap depth from the energy of the bottom of CB (E_C). As reported in previous our paper, E_{Cr2+} in YAGG always

appears near -2.75 eV ± 0.06eV[9]. E_{V2+} and E_{Sc2+} in YAGG were spread near -3.30±0.22 eV and -2.88±0.06eV, respectively. The VRBE of the single electron in the lowest energy 3*d*, 4*d*, and 5*d* levels in group IIIa, IVa, Va and VIa transition metal (TM) and lanthanide (Ln) ions spread ±1 eV around a mean value [20-23]. Therefore, it is regarded that the VRBE of each TM^{2+} in $Y_3Al_{5-x}Ga_xO_{12}$ has the reasonable range. The VRBE of TM^{2+} (TM=Sc, V) slightly increases with increasing Ga content. This is probably because the crystal field splitting of 3*d* transition metal ions becomes much weaker and the t_{2g} state of TM^{2+} shifts higher energy. Also, from the charge transfer energy of 6.67 eV in $Y_3Al_5O_{12}:Sc^{3+}$[24], E_{Sc2+} was reported to be -2.71 eV by Dorenbos, which is the very similar value with the obtained E_{Sc2+} of -2.94 eV from the trap depth. This coincidence also supports that these electron trap levels are due to TM^{2+}.

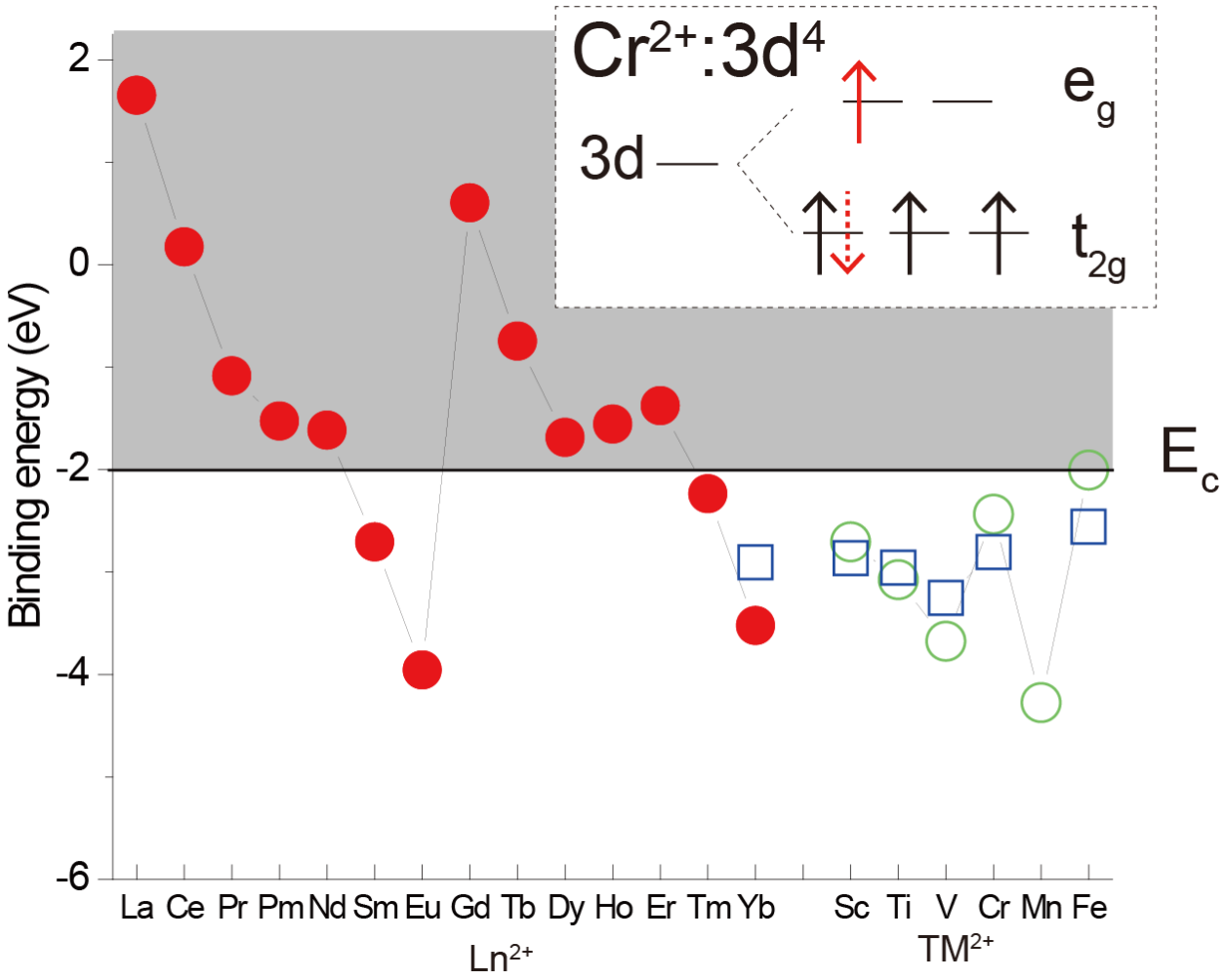

Figure 5. VRBE diagram of Ln^{2+} and TM^{2+} in $Y_3Al_2Ga_3O_{12}$, blue square is estimated from the experimental data of TL, red circle is estimated from the Dorenbos model, green circle is estimated from the DMVE calculation in this work.

Here, the VRBE of TM^{2+} is discussed from the viewpoint of the number of *d* electron, effective nuclear charge and crystal field splitting. Figure 5 shows the VRBE diagram of Ln^{2+} and TM^{2+} in the $Y_3Al_2Ga_3O_{12}$ host. The VRBE of Ln^{2+} (red circles in Figure 5) is referred from the paper by Dorenbos[25, 26], and for the Ln^{2+}, the typical zig-zag curve can be seen. The values of VRBE of TM^{2+} were estimated from two methods: One is from the trap depth, which is calculated by the peak temperature of measured TL glow curve (blue squares in Figure 5 and

E_{TM2+_exp} in Table 2). Another value is estimated by using DVME calculation as discussed later (green circle in Figure 5 and E_{TM2+_cal} in Table 2). The absolute energy of CT energy can be discussed because the calculated energy shows good agreement with the experimental result; for example, the experimental and calculated charge transfer energies from and 6.49 eV, respectively.

For the VRBE of TM^{2+} from the experimental data (E_{TM2+_exp}), when 3*d* electron increases, it does not follow the monotonic increase (or decrease) tendency, but like a zig-zag curve. Although some E_{TM2+_exp} are lacking due to the limitation of material synthesis and thermoluminescence investigation, E_{TM2+_exp} of $3d^1$ (Sc^{2+}), $3d^2$(Ti^{2+}), $3d^3$(V^{2+}), $3d^4$(Cr^{2+}) with the continuous number of 3*d* electrons can be discussed reasonably. The E_{TM2+_exp} decreases with increasing 3*d* electron from Sc^{2+} to V^{2+} and increases at Cr^{2+}. If we consider only the number of 3*d* electrons and effective nuclear charge in free ions, VRBE of TM^{2+} should monotonically decrease from $3d^1$ to $3d^4$. This is because the effective nuclear charge increases in the order of $_{21}$Sc, $_{22}$Ti, $_{23}$V, $_{24}$Cr, which attract electrons strongly with increasing atomic number, and there is no strong electron repulsion due to the less 3*d* electrons than the electrons for the semi-closed shell. To discuss the non-monotonic tendency, we should consider the effect by the crystal field splitting for E_{TM2+_exp} in compounds. The trivalent 3*d* transition metal from Sc^{3+} to Cr^{3+} can occupy the octahedral site in the garnet crystal rather than the tetrahedral site due to the relatively large ionic radius. The electron traps by trivalent 3*d* transition metal (i.e. E_{TM2+}) is also located at the octahedral site. In the octahedral site, the 3*d* energy level splits to t_{2g} (d_{xy}, d_{yz}, d_{yz}) and e_g (d_{z^2}, $d_{x^2-y^2}$) as shown in Figure 5 inset. If the 3*d* electrons are less than 4, all 3*d* electrons occupy the t_{2g} level by the Hund rules. On the other hand, for the $3d^4$ electron configuration of Cr^{2+}, the fourth electron can occupy the e_g level as high spin state or the t_{2g} level as low spin state

as shown in red dot lines in Figure 5 inset. Both the high and low spin state of Cr^{2+} could have the higher energy compared with V^{2+} even if the increase of effective nuclear charge is taken into account. This is because for the high spin state the e_g level accommodating the forth electron is located at higher energy compared with t_{2g} level and for the low spin state the fourth electron at t_{2g} level is affected by strong Coulomb repulsion due to the occupation of two electrons into the same 3*d* orbit.

Table 2. Calculated charge transfer energy of 3*d* transition metal from DVME, E^{CT}_{cal}, the calibrated charge transfer neregy, $E^{CT}_{cal\_calib}$, the estimated VRBE from the DVME calculation in $Y_3Al_5O_{12}$, E_{TM2+_cal}, and the VRBE estimated form TL experimental data in $Y_3Al_2Ga_3O_{12}$, E_{TM2+_exp}.

	E^{CT}_{cal}	$E^{CT}_{cal\_calib}$	E_{TM2+_cal}	E_{TM2+_exp}
Sc	8.40	6.67	-2.71	-2.86
Ti	8.03	6.30	-3.07	-2.96
V	7.43	5.70	-3.67	-3.25
Cr	8.67	6.94	-2.43	-2.80
Mn	6.83	5.10	-4.27	-
Fe	9.10	7.37	-2.00	-2.56

To discuss this hypothesis, the charge transfer energies of TM^{3+} (O^{2-} - $TM^{3+} \rightarrow O^{-}$-$TM^{2+}$) in the $Y_3Al_5O_{12}$ were estimated using Ab initio calculation. The second column of Table 2 is the

charge transfer energy, E^{CT}_{cal}, estimated by DVME calculation with lattice relaxation correction. Since there is a systematic overestimation of the theoretical CT energy, the values are shifted by -1.86 eV, which is estimated from the CT energy (6.67eV) from O^{2-} to Sc^{3+} in $Y_3Al_5O_{12}$ [24], as shown in the third column of Table 2. Then, the VRBE of TM^{2+} was estimated by adding the calculated E^{CT} to the top of VB in $Y_3Al_5O_{12}$ which was reported previously[9]. The VRBE of TM^{2+} in $Y_3Al_2Ga_3O_{12}$ estimated from the trap depth obtained in TL glow curves as shown in Figure 1. From the calculation, it is found that the high spin state of Cr^{2+} is much more stable than the low spin state in the garnet crystal. The estimated VRBE from the calculation, E_{TM2+_cal}, in $Y_3Al_5O_{12}$ can be compared with the E_{TM2+_exp} in $Y_3Al_2Ga_3O_{12}$ because the VRBE of 3*d* transition metal ions in $Y_3Al_{5-x}Ga_xO_{12}$ spread in the narrow region as discussed in Figure 4. As shown in column 4 and 5 of Table 2, the calculated E_{TM2+_cal} is in line with the E_{TM2+_exp} from Sc to Cr. Therefore, the increase of E_{TM2+} at Cr^{2+}:$3d^4$ is confirmed to be caused by the crystal field splitting. The E_{TM2+_cal} of Mn^{2+} decreases significantly because of the semi-closed shell, and the E_{TM2+_cal} of Fe^{2+} increases due to strong Coulomb repulsion of two electrons on the same 3*d* orbit.

4.2. Design of electron (de)trapping phosphors

From the obtained zig-zag curve of TM^{2+}, we can design a new electron trapping materials such as persistent phosphors, photostimulated phosphors and storage phosphors. Figure 6 shows the persistent luminescence decay curves of Ce^{3+} luminescence after 460 nm charging for 5 min in $Y_3Al_2Ga_3O_{12}$:Ce^{3+} and $Y_3Al_2Ga_3O_{12}$:Ce^{3+}-TM^{3+} (TM=Sc, V, Cr). The detrapping rate is determined by $s \times \exp(-E_{trap}/kT)$, so that the persistent decay profile can be controlled by changing the transition metal codopants. In the order of Cr^{2+}, Sc^{2+}, V^{2+}, the trap depth becomes

much deeper as shown in Figure 1. Consequently, the persistent luminescence intensity at ambient temperature is much weaker at beginning, but the persistent luminescence decay slope becomes much gentle as shown in Figure 6. For $Y_3Al_2Ga_3O_{12}:Ce^{3+}$-$V^{3+}$, the trap depth of 1.26 eV is too deep for the persistent luminescence at ambient temperature. However, the deeper trap is suitable for the photostimulated phosphor. Figure 7 shows the luminescence spectrum stimulated by the 980 nm IR laser before and after UV charging in $Y_3Al_2Ga_3O_{12}:Ce^{3+}$-$V^{3+}$. Before charging, there is no luminescence while after charging Ce^{3+}:$5d_1$-$4f$ luminescence was observed by IR-stimulation, which is so-called as photostimulated luminescence. This result clearly shows that $Y_3Al_2Ga_3O_{12}:Ce^{3+}$-$V^{3+}$ with the deeper traps is suitable for photostimulated phosphors. We can successfully demonstrate that TM^{3+} codopnat ions also act as suitable electron traps like co-dopants of trivalent lanthanide ions in persistent phosphors, and open up a new cation combination material group for phosphors related carrier trapping.

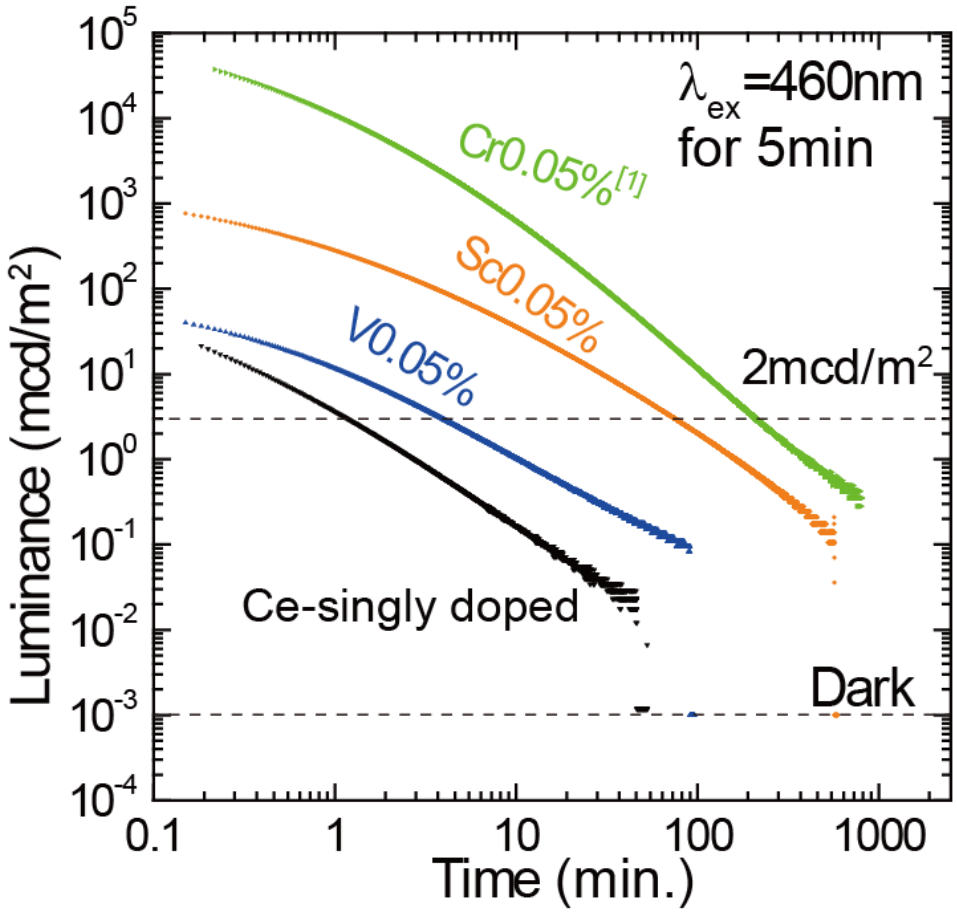

Figure 6. Ce^{3+}:$5d_1$-4f Persistent luminescence decay curves in $Y_3Al_2Ga_3O_{12}$:Ce^{3+}-TM^{3+}(TM=Sc, V, Cr) and $Y_3Al_2Ga_3O_{12}$:Ce^{3+}.

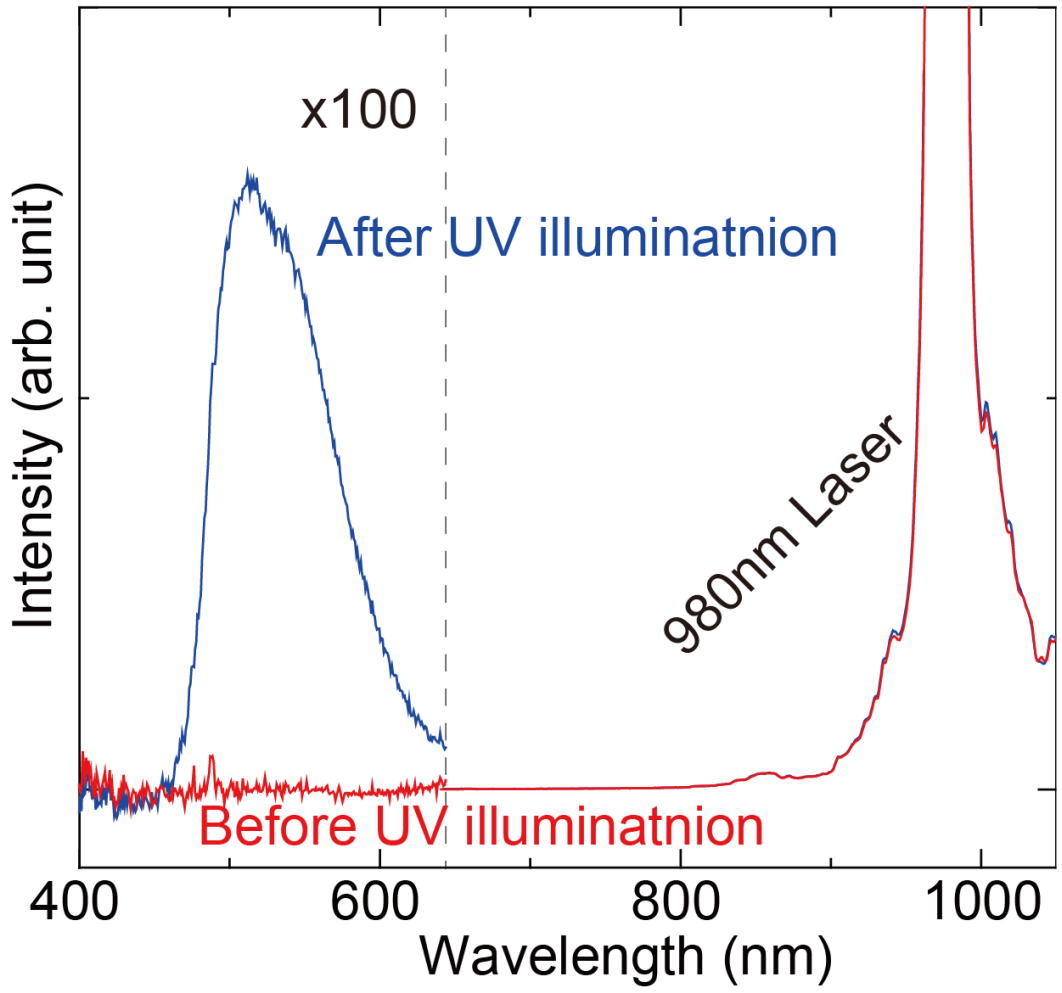

Figure 7. Photostimulated luminescence spectrum by 980 nm before UV charging and after UV charging.

5. Conclusions

Thermoluminescence glow curves in $Y_3Al_{5-x}Ga_xO_{12}:Ce^{3+}$ codoped with 3*d* transition metal ions (TM^{3+}) were investigated. The TL peak temperature is dramatically changed by varying TM^{3+} ion. The electron trap depth in the samples with different 3*d* transition metal ions is totally different from each other. This is because electron trap is formed by 3*d* transition metal ions.

The estimated vacuum referred binding energy of TM^{2+} from trap depth shows a zig-zag curve, which is found to be affected by the number of d electron, nuclear charge and crystal field splitting according to the results by the first-principle calculation. Utilizing the obtained TM^{2+} zig-zag curve, new persistent phosphors of $Y_3Al_2Ga_3O_{12}:Ce^{3+}$-$Sc^{3+}$ and photostimulated phosphors of $Y_3Al_2Ga_3O_{12}:Ce^{3+}$-$V^{3+}$ were successfully developed.

Acknowledgements

This work was supported by JSPS KAKENHI Grant Number 16K05934 and 16H06441.

References

[1] T. Matsuzawa, Y. Aoki, N. Takeuchi, Y. Murayama, J. Electrochem. Soc., 143 (1996) 2670-2673.
[2] M. Sonoda, M. Takano, J. Miyahara, H. Kato, Radiology, 148 (1983) 833-838.
[3] R. Yokota, H. Imagawa, J. Phys. Soc. Jpn., 23 (1967) 1038-1048.
[4] J.H. Schulman, R.J. Ginther, C.C. Klick, R.S. Alger, R.A. Levy, J. Appl. Phys., 22 (1951) 1479-1487.
[5] M. Akiyama, Appl. Phys. Lett., 97 (2010) 181905.
[6] J. Ueda, T. Shinoda, S. Tanabe, Opt. Mater. Express, 3 (2013) 787-793.
[7] J. Ueda, K. Kuroishi, S. Tanabe, Appl. Phys. Express, 7 (2014) 062201.
[8] J. Xu, J. Ueda, K. Kuroishi, S. Tanabe, Scripta Mater., 102 (2015) 47-50.
[9] J. Ueda, P. Dorenbos, A.J.J. Bos, K. Kuroishi, S. Tanabe, J. Mater. Chem. C, 3 (2015) 5642-5651.
[10] J. Ueda, J. Ceram. Soc. Jpn., 123 (2015) 1059-1064.
[11] J. Ueda, K. Kuroishi, S. Tanabe, Appl. Phys. Lett., 104 (2014) 101904.
[12] K. Van den Eeckhout, P.F. Smet, D. Poelman, Materials, 3 (2010) 2536-2566.
[13] K. Van den Eeckhout, D. Poelman, P. Smet, Materials, 6 (2013) 2789-2818.
[14] P. Dorenbos, J. Lumin., 122-123 (2007) 315-317.
[15] P. Dorenbos, J. Electrochem. Soc., 152 (2005) 107-110.
[16] P. Dorenbos, A.J.J. Bos, Rad. Meas., 43 (2008) 139-145.
[17] K. Ogasawara, S. Watanabe, Chapter 22 - Current Situation and Future Development of Discrete Variational Multielectron Method, in: R.S. John, B. Erkki (Eds.) Adv. Quantum Chem., Academic Press, 2008, pp. 297-314.
[18] J.T. Randall, M.H.F. Wilkins, Proc. Roy. Soc. A Math. Phys. Sci., 184 (1945) 390-407.
[19] J.T. Randall, M.H.F. Wilkins, Proc. Roy. Soc. A Math. Phys. Sci., 184 (1945) 365-389.
[20] E.G. Rogers, P. Dorenbos, ECS J. Solid. State Sci. Technol., 3 (2014) R173-R184.
[21] E.G. Rogers, P. Dorenbos, J. Lumin., 153 (2014) 40-45.
[22] E.G. Rogers, P. Dorenbos, J. Lumin., 155 (2014) 135-140.
[23] P. Dorenbos, E.G. Rogers, ECS J. Solid. State Sci. Technol., 3 (2014) R150-R158.
[24] V. Mürk, N. Yaroshevich, Phys. Stat. Sol. b, 181 (1994) K37-K40.
[25] P. Dorenbos, J. Lumin., 134 (2013) 310-318.
[26] P. Dorenbos, ECS J. Solid. State Sci. Technol., 2 (2013) R3001-R3011.

Figure captions

Figure 1. Normalized TL glow curves recorded with 10K/min heating rate of $Y_3Al_2Ga_3O_{12}:Ce^{3+}$-$TM^{3+}$(TM=Sc, Ti, V, Cr, Fe), $Y_3Al_2Ga_3O_{12}:Ce^{3+}$ -Yb^{3+} and $Y_3Al_2Ga_3O_{12}:Ce^{3+}$ after UV charging at 100 K.

Figure 2. Normalized TL glow curves recorded at 10K/min heating rate of $Y_3Al_{5-x}Ga_xO_{12}:Ce^{3+}$-$Sc^{3+}$ with different Ga content x after UV charging at 100 K.

Figure 3. Normalized TL glow curves recorded at 10K/min heating rate of $Y_3Al_{5-x}Ga_xO_{12}:Ce^{3+}$-$V^{3+}$ with different Ga content x after UV charging at 100 K.

Figure 4. Stacked VRBE diagrams of $Y_3Al_{5-x}Ga_xO_{12}$ for TM^{2+} (TM=Sc, V, Cr).

Figure 5. VRBE diagram of Ln^{2+} and TM^{2+} in $Y_3Al_2Ga_3O_{12}$, blue square is estimated from the experimental data of TL, red circle is estimated from the Dorenbos model, green circle is estimated from the DMVE calculation in this work.

Figure 6. Ce^{3+}:$5d_1$-4f Persistent luminescence decay curves in $Y_3Al_2Ga_3O_{12}:Ce^{3+}$-$TM^{3+}$(TM=Sc, V, Cr) and $Y_3Al_2Ga_3O_{12}:Ce^{3+}$.

Figure 7. Photostimulated luminescence spectrum by 980 nm before UV charging and after UV charging.

Table captions

Table 1. Temperature maximum, Tm, of TL glow curves recorded at 10 K min^{-1} heating rate, the trap depth, E^{trap}, and VRBE of Sc^{2+}, V^{2+} and Cr^{2+} (E_{Sc2+}, E_{V2+} and E_{Cr2+})

Table 2. Calculated charge transfer energy of 3d transition metal from DVME, E^{CT}_{cal}, the calibrated charge transfer energy, $E^{CT}_{cal\_calib}$, the estimated VRBE from the DVME calculation in $Y_3Al_5O_{12}$, E_{TM2+_cal}, and the VRBE estimated form TL experimental data in $Y_3Al_2Ga_3O_{12}$, E_{TM2+_exp}.